UPSTREAM DISTURBANCES INDUCED BY AN ORIFICE PLATE ON A HORIZONTAL GAS-LIQUID MIXTURE FLOWING ON THE SLUG REGIME

Nathan da Costa Maidana, nathan@fem.unicamp.br
Eugênio Spanó Rosa, erosa@fem.unicamp.br
Faculty of Mechanical Engineering - State University of Campinas, Rua Mendeleyev 200, 13083-860, Campinas, SP, Brazil

Abstract. *The horizontal slug flow through orifice plates is analyzed through the influence of orifices' sizes on the upstream slug flow structure. It is expected that the alternate passage of liquid slugs and liquid films associated to elongated bubbles will cause an intermittent pressure difference at the orifice which will propagate upstream disturbing the velocities, the lengths, the frequency of passage and above all the slug formation. The experimental study is carried on a horizontal air-water flow on the slug regime through an orifice plate. The test section consists of a transparent acrylic pipe with 26 mm ID and 26.24 m long. The orifice plate is placed at 632 pipe diameters downstream the inlet. Three orifices are tested with area contraction ratios of 0.250, 0.123 and 0.072. Measurement of the pressure fluctuations, the instantaneous void fraction as well as the lengths and velocities of the slugs are taken at the test section. The analysis of the experimental data discloses how the slug flow properties are changed due to an area obstruction by comparing with the data of a straight pipe without area contraction.*

Keywords: *slug flow, orifice plate, pressure difference, void fraction, air-water*

1. INTRODUCTION

The two-phase flow behavior of a gas liquid mixture through valves, nozzles, orifices, pipe contractions or expansions and other pipe singularities is important for the control and operation of commonly found on power generation plants, refrigeration units, chemical reactors, depressurization emergency systems and on gas-oil production lines found on the petroleum industry.

The flow acceleration induced by a pipe singularity due to an area change continuously deforms the interfaces exhibiting an ever-changing void fraction near the singularity and back propagate pressure pulses upstream the obstruction disturbing the flow structure as well. The design and control of pipe singularities that change the flow area require models to evaluate the pressure losses and the knowledge of the upstream and downstream effects on the gas-liquid flow properties, including the phase distribution and velocities.

Some works approached the gas-liquid mixture flowing through orifices with reference only to the pressure drop regardless the flow pattern or the influence of the singularity on the two-phase flow structure. Chisholm (1983) develops pressure drop models based on the separated phase's models with and without slip, employing two-phase multipliers and compares against experimental data. Salcudean et al. (1983) analyzed pressure drop in various forms of flow obstruction geometries. Lin (1982) developed a model for flow measurement of gas-liquid flows using water and steam data and Kosajoy et al. (1997) developed a pressure drop model for a plate with multiple orifices and compare against R-113 experimental data. More recently, Fossa and Guglielmini (2002) developed a model to predict the pressure drop in orifices and compares against an air-water database with void fraction spanning from 20% up to 85%. The singularity were at 100D to 150D downstream the inlet. Oliveira et al. (2009) developed a comparative study among different models for mass measurements in gas-liquid flow based on orifices and compared against an air-water experimental data basis identifying the flow regime. The experimental data came from a test section with 0.021 m ID and the singularities were at 75D downstream the inlet.

There are quite a few numbers of works addressing to the flow structure in area contractions (Schmidt and Friedel, 1997; Fossa and Guglielmini, 1998; Bertola, 2004 and Chen et al., 2008) or in area expansions (Patrick and Swanson, 1959; Aloui et al., 1999; Ahmed, 2007), but the number of works addressed to the flow structure through orifices is reduced. Fossa et al. (2006) gives details of the flow structure of a horizontal air-water slug flow in the presence of an orifice plate. The test section is a 40mm ID pipe with 300D long. The concentric orifices have an area contraction ratio, $\sigma = (d/D)^2$, in respect to the orifice diameter, d, of 0.74 and of 0.54 and are made with three different plate thicknesses. Using a multiple ring impedance sensor, the average void fraction was mapped upstream and downstream at distances up to 4D of the orifice edges. It was found that the void fraction peaks just downstream the orifice edge, furthermore the peak value increases as the orifice area contraction ratio decreases. In addition, it was observed that the slug frequency slightly decreases for low contraction area ratios as the mixture velocity increases. Zeghloul et al. (2015) explored the effect of an orifice on the upward air-water flow at the bubbly, slug and churn regimes. The vertical test section has 34mm ID and the orifice plate is installed at 121D downstream the inlet. The presence of the orifice changes significantly the flow structure at the neighborhood of the singularity, but the flow recovers the upstream condition about 20D, 10D and 7D to bubbly, slug and churn regimes. The frequencies of the periodic structures are very similar upstream and downstream of the orifice for bubbly and slug regime.

The present work addresses to the flow disturbances induced by an orifice plate installed at 632 D downstream the mixer in a horizontal air-water slug flow. The motivation is toward to a better understand of the slug flow structure, to assist the development of models to predict the pressure drop in pipe singularities with area change. The approach is experimental consisting of measurements of the pipe cross section void fraction and of the pipe axial pressure distribution in conjunction to the slug flow properties such as elongated bubble velocity, liquid slug and film length and frequency of passage. The analysis employs averaged data, probability density functions and power spectral densities to disclose the flow structure disturbances upstream the orifice plate.

2. EXPERIMENTAL PROCEDURE AND DATA PROCESSING

The horizontal experimental test section has a 26 mm ID straight pipe made of transparent acrylic with 26.24 m long or 1009 D, see Figure 1. The working fluids are compressed air and water at ambient conditions, nearly 93.7 kPa and 25 ºC. The water density and viscosity are 998 kg/m^3 and 0.001 Pa.s, while the air was treated as an ideal gas with R equals to 286.9 J/kgK. Three compressors and a centrifugal pump supply the air and the water to the mixer installed at the entrance of the test section. The air and the water flow rates are measured separately employing a homemade sonic nozzle and a Metroval Coriolis mass type flow meter respectively. The air-water mixer consists of a pipe section divided in two by an internal split plate. The water is injected at the bottom section while the air is injected at the top section. The air and the water streams flow in parallel at a distance equivalent to ten pipe diameters before mixing. At the end of the test section, the air-water mixture is discharged into a receiving tank with 3 m^3 in volume opened to the atmosphere. The air vents to the atmosphere and the liquid, free of air bubbles, is pumped back to the test section.

The test section has four measuring stations identified by S1, S2, S3 and S4 respectively located at 153 D, 307 D, 551 D and 870 D downstream the air-water mixer. The orifice plate is located at 632 D downstream the mixer, positioned at 81 D downstream S3 and 238 D upstream S4. Three orifice plates with throat diameter, d, made of stainless steel are used with area contraction ratio, $\sigma = (d/D)^2$, of 0.250, 0.123 and 0.072. Each orifice is a concentric circular hole, with squared edges with thickness, t, of 3 mm. The thickness to orifice diameter ratio, t/d, is of 0.231, 0.330 and 0.429, which result in thin orifice plates accordingly to Chisholm (1983). A differential pressure transducer Smar LD301 measures the pressure difference at the orifice plate through flange taps, at the upstream and downstream faces of the plate.

Each measuring station has a Smar LD301 pressure transducer and a twin set of house-made single wire conductive probes axially spaced of 112.5 mm. The conductivity probes have an output voltage, V_m, which spans between low and high values, V_{low} and V_{high}. These extremes, V_{low} and V_{high}, correspond when the test section is full of gas or full of liquid, respectively. Defining the dimensionless voltage, V^*, as:

$$V^* = \frac{V_m - V_{low}}{V_{high} - V_{low}} \tag{1}$$

it is possible to show that the equivalent liquid film height, h_f, is proportional to (1 – V*), Rosa et al. (2010).

The conductive probes have an output dimensionless voltage, 1-V*, proportional to the cross section's void fraction of the air-water flow. The exact dependence between V* and the dimensionless liquid film thickness, h_f/D, is determined experimentally through a calibration curve. The dimensionless output voltage signal is mapped into the liquid film heights. The air-water interface at the elongated bubble behaves as a flat surface because the gas and liquid velocities are low. Furthermore, visual observations disclosed that the liquid slugs are not aerated. Based on this assumption, the geometrical relationship between the film height and the void fraction (Taitel and Barnea, 1990) is given as:

$$\alpha = 1 - \frac{1}{\pi}\left\{\pi - A\cos\left[2\left(h_f / D\right) - 1\right] + \left[2\left(h_f / D\right) - 1\right]\sqrt{1 - \left[2\left(h_f / D\right) - 1\right]^2}\right\} \tag{2}$$

The intermittence of the slug flow is captured by the twin set of conductance probes as square waves in V* shifted in time due to the probes' spacing. A detailed description of the conductive probes is in Rosa et al. (2010). The analogical signals of the twin conductance sensors and of the pressure at each measuring station are sampled at 3 kHz through a channel multiplexer and digitized employing, respectively, a SCXI-1600 and a SCXI-1308 models, both from National Instruments.

During the preliminary tests of the experimental apparatus, it was observed large pressure pulses back propagated from the orifice plate, which caused fluctuations on the air and water inlet flow rates. To avoid the undesired inlet fluctuations two procedures were adopted, the use of a sonic nozzle to measure the air flow rate and operate the centrifugal pump at the maximum speed and use an inlet choke to set the desired water flow rate. A quite stable inlet air flow rate was obtained operating with the choked nozzle. The large pressure drop at the inlet choke of the water line minimized the inlet water fluctuations to less than 4% of the nominal flow rate.

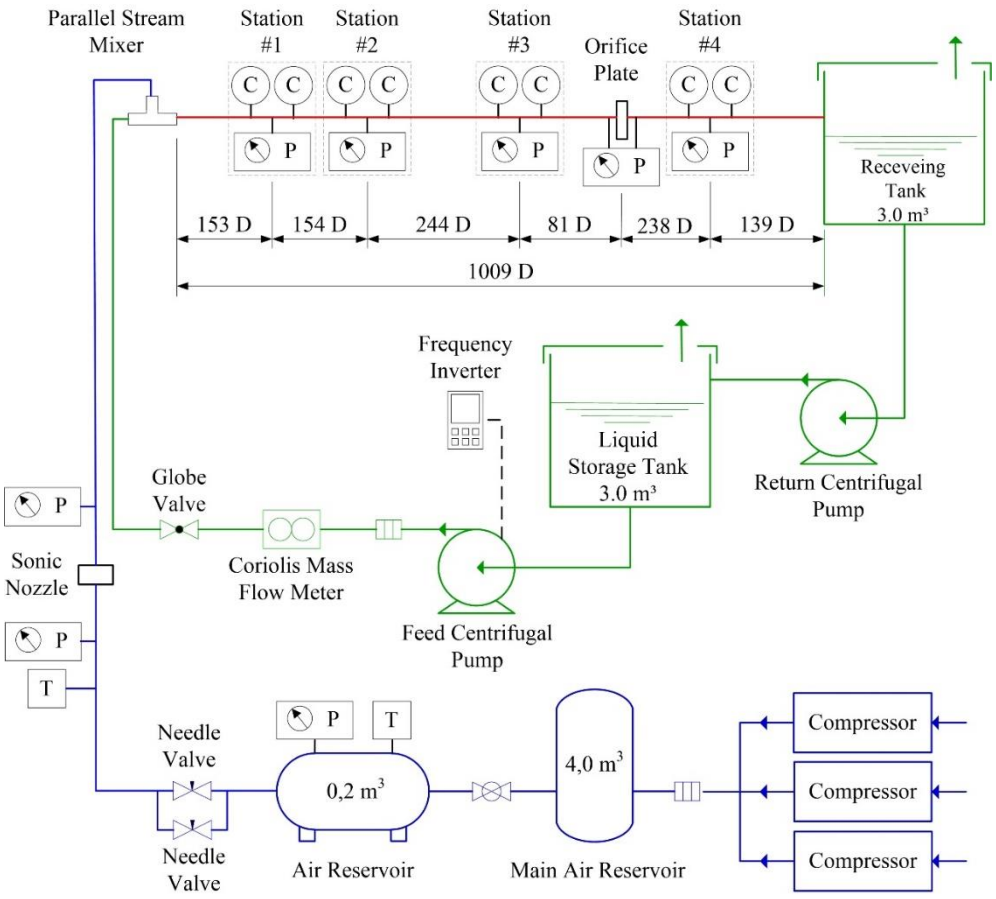

Figure 1. Schematic of the experimental apparatus and test section. (adapted from Dalla Maria, 2016)

The inlet water and air flow rates are expressed in terms of their superficial velocities, J_L and J_G defined as the ratio of the volumetric phase flow rate by the pipe cross section area. The nominal air and water superficial velocities were (J_L, J_G) of (0.30m/s, 0.30m/s) and (0.30m/s, 0.50m/s). The chosen values assure long bubbles with a mean length spanning from 50D to 140D. An increase on the gas flow rate would lead to larger bubbles and the test section would have few bubbles to be representative of the bubble-to-bubble interaction of slug flow.

The test grid, shown in Table 1, consists of four series. The first employs a straight pipe without orifice plate used as a reference state and the other three series correspond to each orifice plate with area contraction ratio, σ, of 0.250, 0.123 and 0.072. Each series consists of 10 runs for each pair of water and air superficial velocities. The experimental work amounts to 80 runs. Each individual run has the liquid and gas inlet flow rates carefully adjusted to nominal values. Before starting the data acquisition, it is necessary to give a time delay of nearly 30s until the effects of the changes on the inlet flow rates exits the test section. The data acquisition last for 120 s at a sampling rate of 3000 samples per second. The sampling data consist of 13 channels corresponding to the pressure and the twin signal of the conductive probes for measuring stations #1 to #4 plus the orifice plate pressure difference.

The following data processing procedures apply to a single experimental run. The first step is to transform the output voltage signals of the pressure transducers and conductance probes into Pascal and a dimensionless voltage, V*. Both P and V* are analog signals which are digitized by the acquisition system at a sampling rate of 3000 samples per second to build the (t,P) and (t, V*) time series. The pressure values come from the transducer calibration curve. This step produces five time series (t, P) corresponding to each pressure transducer installed along the test section plus the one at the orifice plate flange taps. The conductance sensors dimensionless voltage, see Eq (1), is assembled with V_{high} and V_{low} from the sensors' calibration data. Similarly to the pressure transducers, this step produces eight time series (t, V*) corresponding to each sensor located at each measuring station. The data processing of the twin sensors' time series gives the film height, h_f/D, and the pipe cross section void fraction.

Table 1. Test grid. The first and second columns show the area contraction ratio and the measuring stations. The number of slug units and the liquid and gas superficial velocities for each station.

Area Contraction Ratio	Meas. Station	Units	J_L	J_G	Units	J_L	J_G
		-	m/s	m/s	-	m/s	m/s
σ = 1.0 No Orifice	#1	946	0.30	0.30	939	0.30	0.49
	#2	836	0.30	0.30	789	0.30	0.50
	#3	688	0.30	0.31	649	0.30	0.50
	#4	562	0.30	0.31	618	0.30	0.51
σ = 0.250	#1	309	0.30	0.30	595	0.30	0.49
	#2	437	0.30	0.30	591	0.30	0.49
	#3	450	0.30	0.31	508	0.30	0.50
	#4	362	0.30	0.31	445	0.30	0.51
σ = 0.123	#1	350	0.30	0.30	474	0.30	0.48
	#2	369	0.30	0.30	428	0.30	0.48
	#3	306	0.30	0.31	359	0.30	0.49
	#4	287	0.30	0.33	389	0.30	0.53
σ = 0.072	#1	339	0.30	0.30	456	0.30	0.49
	#2	327	0.30	0.30	401	0.30	0.49
	#3	238	0.30	0.31	309	0.30	0.51
	#4	349	0.30	0.37	355	0.30	0.62

Further processing the twin sensors' time series, it is possible to determine the bubble nose time of flight between the upstream and downstream probe and the residence time of each phase in contact with the sensors. Additional data processing on the time of flight and on the residence time will give the features of each slug unit crossing the sensors. The bubble's nose velocity of each individual elongated bubble, u_T, is determined by the ratio between the twin sensor spacing, S, and the time of flight to the bubble nose to move from rear to the front sensor. The lengths of each liquid film, L_f , as well as of each liquid slug, L_S, are determined by multiplying the residence time of the corresponding liquid film or liquid slug to the bubble nose velocity. The intermittence factor, β, of each unit is defined as: $\beta = L_f/(L_f+L_S)$. The frequency of passage of each slug, f, is defined as the ratio between the bubble nose velocity and the sum of the lengths of liquid film and the liquid slug. Lastly, a measure of the degree of interaction between neighboring bubbles is accessed estimating the coalescence rate defined as:

$$C(x) = -\frac{1}{N_{b,u}} Lim_{\Delta x \to 0}\left(\frac{N_{b,d} - N_{b,u}}{\Delta x}\right) \equiv -\frac{1}{N_{b,u}}\frac{dN_b}{dx} \tag{3}$$

where $N_{b,d}$ and $N_{b,u}$ represent the total number of bubbles, at a given time interval, crossing the downstream and the upstream pipe cross section spaced Δx from each other. Experimentally, is not possible to determine C(x) as $\Delta x \to 0$, but its average value, C_{av}, for pipe cross sections spaced by a finite distance ΔL is evaluated as:

$$C_{av}(\bar{x}) = -\frac{Ln\left(N_{b,d} / N_{b,u}\right)}{\Delta L} \tag{4}$$

Before closing this section, it is necessary to recognize that the data processing stage has two discrete variables: the pressure and the film height which are sampled at time intervals of 1/3000 s. The cross section void fraction, α, is derived from the film height and is also considered as a discrete variable. Post processing the film height it is possible to define the slug flow properties: u_T, L_f/D, L_S/D and f for each slug unit, which is defined as a liquid slug trailed by an elongated bubble flowing over a liquid film. We refer to these variables as pseudo-discrete, because they are properties associated to each slug unit that crossed the measuring stations; they are not sampled at every 1/3000 sec but just at the instants when the bubble nose crosses the sensors.

3. EXPERIMENTAL RESULTS

To access the influence of orifice plates on the slug flow properties, it is developed a comparative analysis employing as reference the data from flow on a straight pipe without orifice. The results section is structured into five subsections addressing to: the pressure, the void fraction, the slug frequency, the bubble nose translational velocity and lastly, to the liquid film and liquid slug lengths. To support the analysis to be developed on the next sections and for referencing purposes, Table 2 is presented next with the average slug flow properties. The table has two rows and two columns where the orifice contraction ratio and the phases' superficial velocities are identified on the top line and on the first column of each cell, respectively. The table shows the experimental data along the measuring stations, here identified by their axial pipe positions z/D. The average data on u_T, L_f/D, L_S/D, absolute pressure, f, C_{av} and α are presented. Lastly, the average pressure difference measured at the flange taps of the orifice is also presented. The C_{av} unit is in percentage of coalesced bubbles between neighboring measuring stations per meter of pipe, see Eq. (4). Furthermore, the table's line corresponding to S1 indicates a C_{av} value representing the percentage of bubbles that coalesced per meter of pipe between S1 and S2 stations and so on for the next line. The C_{av} is evaluated between S3 and S4 only for the reference flow but it doesn't apply to flows with orifice plate.

Table 2. Average slug flow properties. The data is presented in four clusters accordingly to the orifice area contraction ratio. The columns display the bubble nose translational velocity, the lengths of the liquid film and liquid slug, the pressure, the slug frequency, the coalescence rate, the cross section void fraction and the orifice's pressure difference.

		σ = 1.000							σ = 0.250						
J_L-J_G	z/D	u_T	L_f/D	L_S/D	P	f	C_{av}	α	u_T	L_f/D	L_S/D	P	f	C_{av}	α
m/s	-	m/s	-	-	kPa	Hz	%/m	-	m/s	-	-	kPa	Hz	%/m	-
0.3-0.3	153	0.84	24.1	11.9	96.2	1.02	7%	0.30	0.69	36.6	15.1	97.5	0.71	15%	0.29
	307	0.76	24.0	16.9	95.8	0.78	3%	0.35	0.69	40.7	27.5	97.2	0.40	0%	0.34
	551	0.77	29.8	21.0	94.8	0.63	2%	0.37	0.71	42.7	28.7	95.8	0.39	-	0.32
	870	0.79	36.6	25.8	94.1	0.52	-	0.39	0.67	39.3	20.9	93.9	0.53	-	0.34
	ΔP Orifice	-	-	-	-	-	-	-	-	-	-	3.2	-	-	-
0.3-0.5	153	0.95	31.7	11.1	96.6	0.93	6%	0.43	0.91	47.9	13.5	98.2	0.64	3%	0.43
	307	0.95	38.4	15.6	96.2	0.74	3%	0.48	0.92	50.3	17.5	97.8	0.57	3%	0.46
	551	0.96	47.9	18.8	95.0	0.59	1%	0.49	0.91	59.1	19.2	96.5	0.49	-	0.46
	870	0.95	50.4	19.8	94.2	0.56	-	0.52	0.95	64.3	17.5	93.8	0.53	-	0.52
	ΔP Orifice	-	-	-	-	-	-	-	-	-	-	4.0	-	-	-

		σ = 0.123							σ = 0.072						
J_L-J_G	z/D	u_T	L_f/D	L_S/D	P	f	C_{av}	α	u_T	L_f/D	L_S/D	P	f	C_{av}	α
m/s	-	m/s	-	-	kPa	Hz	%/m	-	m/s	-	-	kPa	Hz	%/m	-
0.3-0.3	153	0.82	42.6	11.2	103.9	0.98	4%	0.34	0.91	42.7	10.1	117.8	1.03	1%	0.37
	307	0.82	42.1	16.4	103.8	0.84	4%	0.39	0.92	46.5	12.6	117.9	0.99	1%	0.40
	551	0.87	66.7	20.0	101.9	0.63	-	0.42	1.03	65.5	14.6	115.1	0.95	-	0.41
	870	0.97	64.7	17.5	94.8	0.85	-	0.44	1.30	64.4	23.5	95.2	1.11	-	0.51
	ΔP Orifice	-	-	-	7.4	-	-	-	-	-	-	13.1	-	-	-
0.3-0.5	153	1.01	56.6	13.2	104.7	0.78	3%	0.46	1.13	59.0	13.2	120.1	0.87	1%	0.47
	307	1.02	61.2	19.0	104.6	0.69	1%	0.49	1.24	72.3	19.0	120.2	0.83	-2%	0.49
	551	1.21	99.9	22.7	102.6	0.63	-	0.54	1.66	138.9	21.0	117.0	0.93	-	0.57
	870	1.26	82.6	27.6	94.4	0.74	-	0.56	1.94	122.0	24.1	95.3	1.31	-	0.64
	ΔP Orifice	-	-	-	9.4	-	-	-	-	-	-	16.8	-	-	-

3.1 The Pressure

The pressure data is on Figure 2. The information is shown using five rows and two columns. The left and right columns refer to pressure data taken with the phases' velocities (J_L, J_G) of (0.30, 0.30) m/s and (0.30, 0.50) m/s, respectively. The top row displays pressure traces at the orifice plate, followed by the absolute pressure at S3 and S1 for orifices with σ of 0.250 and 0.072, labeled as (a) and (b), respectively. The 2nd row shows the average absolute pressure along the test section, measured by S1 through S4; the dashed line represents the axial position of the orifice plate. The 3rd, 4th and 5th rows display the power spectral density, PSD, of the ressure difference at the orifice followed by the PSD of the absolute pressures at S3 and S1 for orifices with σ of 0.250, 0.123, 0.072, respectively.

Starting at the first row, it is observed that the pressure difference at the orifice exhibits high and low values due the occurrence of a mixture with low and high void fractions. If the gas flow rate is increased, it is observed that the amplitude of the pressure difference increases and the same occur for the absolute pressure's fluctuations at S3 and S1. A visual inspection on the pressure signals discloses the signals' crests and valleys roughly matching the pressure difference and the absolute pressure at S3 and S1. For referencing purposes S3 and S1 are at 81D and 479D upstream the orifice plate.

The second row on Figure 2 displays the average absolute pressure along the test section axial position. The straight pipe exhibits the lowest pressure records along the test section as expected. Considering the pressure data upstream the orifice plate, the pressure records for σ of 0.250, 0.123 and 0.072 present a pressure increase in regard to the straight pipe of 1%, 8% and 22% for (J_L,J_G) of (0.30, 0.30) m/s and of 2%, 8% and 24% for (J_L,J_G) of (0.30, 0.50) m/s. Nevertheless, for a constant (J_L,J_G) the pressure gradient is nearly the same regardless the pipe has orifice or not. Also, keeping the orifice area contraction constant but increasing the mixture flow rate, it is observed that the differences among the absolute pressure reading increase.

The PSD of the pressure signals on the 3rd, 4th and 5th rows disclose the dominant frequencies. The orifice with σ of 0.250 has a single dominant frequency of 0.38 Hz and of 0.47 Hz for (J_L,J_G) of (0.30, 0.30) m/s and (0.30, 0.5) m/s respectively. These frequencies suggest that the pressure pulses generated by the alternate passage of liquid slugs and liquid films through the orifice propagate upstream inducing the same frequency to the absolute pressure signals at S3 and S1. Surprisingly, these dominant frequencies are coincident with the mode frequency of the passage of the slugs; see Figure 4, 2nd and 3rd rows, from top to bottom. This topic will be returned in section 3.3. The spectrum of frequencies of the pressure difference at the orifice as well as the spectrum of the absolute pressures become larger and increases in power as the orifice contraction ratio decreases to σ of 0.123 and 0.072. The origin of a wider frequency spectrum at the orifice is a signature that the slug flow structure is changing as the flow approaches the orifice. The absolute pressure at S3, the nearest station upstream the orifice plate, contains most of the dominant frequencies of the spectrum at the orifice. The absolute pressure at S1, the farthest station upstream the orifice, the influence of the orifice weakens, the power of the signal diminishes and the range of frequencies narrows, indicating that the pressure pulses propagating upstream of the orifice are being dissipated.

3.2 The Void Fraction

The dimensionless liquid film height, h_f/D, and the average cross section void fraction are on Figure 3. The figure displays the graphics using four rows and two columns. The left and right columns refers to data taken with the phases' velocities (J_L, J_G) of (0.30, 0.30) m/s and (0.30, 0.50) m/s, respectively. The top row displays traces of the h_f/D at S3 for the reference flow, σ of 1.0, followed by the flows with the orifices with σ of 0.250, 0.123 and 0.072 as indicated on the figures. The 2nd row shows the average void fraction along the test section axial length. The 3rd and 4th rows show the PDFs of the void fraction at S1 and S3 respectively.

The trace of h_f/D for the reference flow, σ of 1.0, is at 81 D upstream of the orifice plate position. The trace displays a non-aerated liquid piston (when h_f/D is 1) trailed by elongated bubble flowing over a liquid film with h_f diminishing up to the long bubble tail. The long bubble tail is in form of a staircase (not plug type). Focusing on the left column, i.e. (J_L, J_G) of (0.30, 0.30) m/s, a slight change is observed on the h_f/D trace regarding to the reference trace for an orifice with σ of 0.250. The changes occur on the liquid film profiles and on the bubble tail's shapes. In addition, it is clearly visible that the liquid slug lengths have increased; see quantitatively the L_S increase on Table 2. For the orifice with σ of 0.123 the changes are more noticeable. The liquid film has and irregular shape with high frequency surface waves. The changes on the h_f/D are even greater for orifices with σ of 0.072. The liquid film and the liquid slug are barely identified. The liquid slugs have big bubbles within them and are not distinguishable the film and the bubble tail. The changes on the h_f/D for the right column, i.e. for (J_L, J_G) of (0.30, 0.50) m/s, are similar to the ones found on the left column but less intense. For orifice with σ of 0.250, the changes on the traces are minimal if compared against the reference trace. When the orifice is changed to σ of 0.123, the trace becomes irregular but it is not observed waves with high frequency on the liquid film. For orifice with σ of 0.072, it is observed the formation of high frequency waves on the liquid film. The rise of high frequency waves on the liquid films are due the reflected pressure waves from the incident slug flow over the orifice. As pressure wave fronts are transmitted upstream they cause small pressure differences on the liquid film inducing changes on the liquid film height.

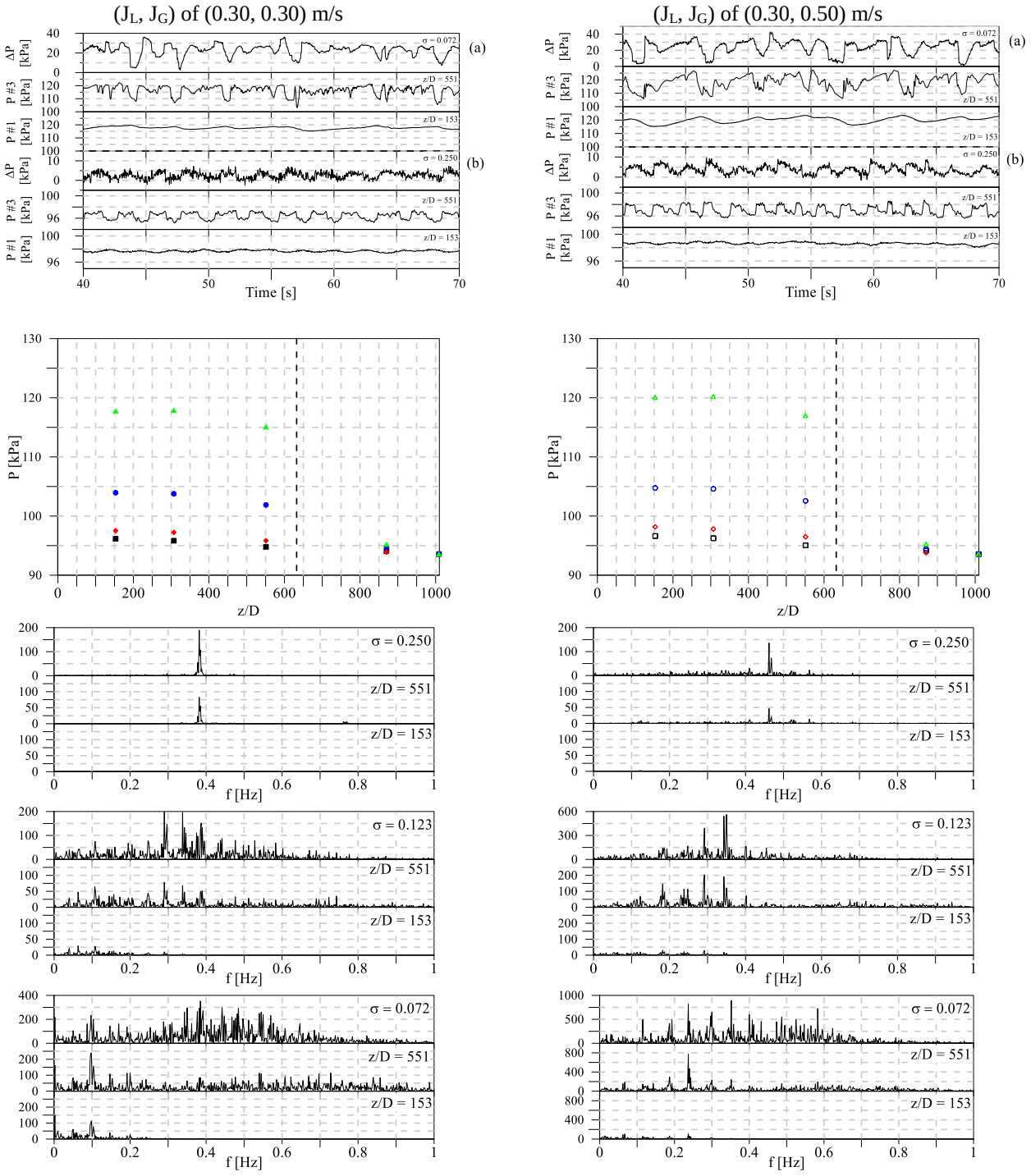

Figure 2. Pressure signals. From top to bottom rows: traces of the orifice plate pressure difference and of the absolute pressures at S3 and S1 for σ of 0.072 (a) and 0.250 (b); average pressure difference along the test section; the next three rows display the PSD of the orifice plate and of the absolute pressures at S3 and S1 for orifices with σ of 0.250, 0.123 and 0.072 respectively. The symbols and/or the colors □, ◊, o, Δ correspond to area contraction ratios of 1, 0.250, 0.123 and 0.072 respectively.

The void fraction average value along the test section is shown on the 2nd row of Figure 3. Focusing on the analysis upstream of the orifice plate, one finds that the presence of orifices with distinct area contraction ratios have influence on the average void fraction. The following void fraction comparisons are drawn based on the reference void fraction data with no obstruction, σ of 1.0. The data for orifice with σ of 0.250 follows the reference void fraction at S1 and S2, but become lower than the reference for S3. Orifices with σ of 0.123 and 0.072 have similar void fraction profiles

between themselves from S1 up to S3, but they are above the reference void fraction data. The average void fraction employing the drift flux model (Zuber and Findlay, 1964) is estimated by the following equation:

$$\alpha = \frac{J_G}{C_0 J + C_\infty \sqrt{gD}} \tag{5}$$

Considering that J_L, J_G, and J are fairly constant from S1 to S3, see data in Table 1, it is possible to foresee that the distribution and the drift coefficients, C_0 and C_∞, are dependent on orifice area contraction ratio. Since the superficial velocities stay constant upstream the orifice plate, it is possible to conclude that the source of void fraction differences is due to the interference of the pressure pulses back-propagated from the orifice. In particular, to σ of 0.250, these pulses changed the slug initiation leading to a high coalescence rate of 15% of bubbles per meter of pipe between S1 and S2, see data in Table 2. The high coalescence rate allowed the flow to become fully developed in a short distance, exhibiting the slug flow properties L_f/D, L_S/D, f and α with no significant change from S2 to S3, see data in Table 2.

The probability density functions for the cross section void fraction at S1 and S3 are on the 3rd and 4th rows. The analysis starts with the left column data for (J_L, J_G) of (0.30, 0.30) m/s. The reference PDF for σ of 1.0 has three mode values: 0, 0.10 and 0.45 which are attributed to the non-aerated liquid slugs, to the bubble tail with stair case shape and to the long bubble body, respectively. These features were already observed on the h_f/D traces on Figure 3, 1st row. For orifices with σ with 0.250, 0.123 and 0.072 the α PDFs only exhibit a bimodal behavior. The presence of the orifice has a tendency to spread the void fractions more uniformly, this is clearly observed for the void fraction PDF at S3 (the 4th row). Focusing on the right column data corresponding to (J_L, J_G) of (0.30, 0.50) m/s, bimodal PDFs are observed with the mode associated to the high α exhibiting positive skew. The increase on the gas superficial velocity reveals the influence of the orifice area contraction ratio more clearly; the decrease on σ displaces the high mode value to the right with a tendency to diminish the high mode toward a uniform distribution.

3.3 Frequency of Passage

The frequency of passage is evaluated by taking the inverse of the period of each slug unit which crossed the conductive sensors at S1 through S4. Since the frequency is not sampled at regular intervals, it is referred as a pseudo-discrete variable. Table 1 shows the number of slug units samples for each station. An alternative to express the frequency of one unit is taking the ratio between the bubble nose velocity to the length of the unit:

$$f_k = \frac{u_{T,k}}{L_{f,k} + L_{S,k}} \qquad 1 \le k \le N \tag{6}$$

where N is the total number of units sampled and k is an index identifying the k^{th} u_T, L_f and L_S.

The frequency of passage is presented on Figure 4 and Figure 5. The Figure 4 displays the information using three rows and two columns. The left and right columns of Figure 4 and Figure 5 refers to data taken with the phases' velocities (J_L, J_G) of (0.30, 0.30) m/s and (0.30, 0.50) m/s, respectively. The top row of Figure 4 displays the average frequency of passage along the test section axial length and the 2nd and 3rd rows show PDFs of the frequency of passage for σ of 1.0, 0.250, 0.123 and 0.072 for S1 and S3 respectively. The Figure 5 shows two rows with the comparative PSD of the pressure difference at the orifice and the PSD of the h_f/D at S3 and S1.

The average frequency of passage along the axial length of the test section is on the top row of Figure 4. The following analysis applies to upstream data of the orifice plate from S1 through S3. The reference case with no orifice is analyzed first exhibiting an average frequency decaying along the test section. This behavior is expected considering the bubble to bubble interaction due to the wake effect (Talvy et al. 2000). The slug flow at S1 is just formed and the lengths of the liquid piston and the liquid films are short. The elongated bubble with faster velocity may overtake its upstream neighbor causing bubble coalescence. The coalescence phenomenon results in a larger bubble and larger liquid slug since the liquid of the small slug separating the two neighboring bubbles is transferred to its downstream neighbor. An observation of the data on Table 2 discloses the L_f/D and L_S/D increasing at a rate faster than the bubble nose velocity, leading to a decaying frequency. Furthermore, the changes on L_f/D and L_S/D are due to the coalescence rate which is accessed through the C_{av}. Notice that for high values of z/D the C_{av} decays and the slug flow properties remain almost stable. The influence of the area contraction ratio on the average frequency of passage may lead to an increase or decrease in regard to the reference frequency (σ of 1.0) and this order may change if z/D increases.

The PDFs of the slug frequencies for S1 and S3 are shown on the 2nd and 3rd rows of Figure 4. A visual inspection discloses a bimodal PDF for the reference void fraction (σ = 1.0) at S1 weakening the physical representativeness of the average value for this case. The presence of the orifice turns the PDF positive skewness. The exception applies to the orifice with σ of 0.250 at S3 on the left column where the PDF is almost symmetrical with high kurtosis. This is a clear footprint that the slug flow reached the stationary state as mentioned before. For all cases the influence of the orifices

was to displace the mode value to the left in regard to the reference PDF (σ of 1.0). Comparing the PDFs at S1 for both columns it is clear the interference of the orifice at the flow. The flow interference is linked to action of the pressure pulses on the slug initiation process since S1 is just 153 D downstream the inlet.

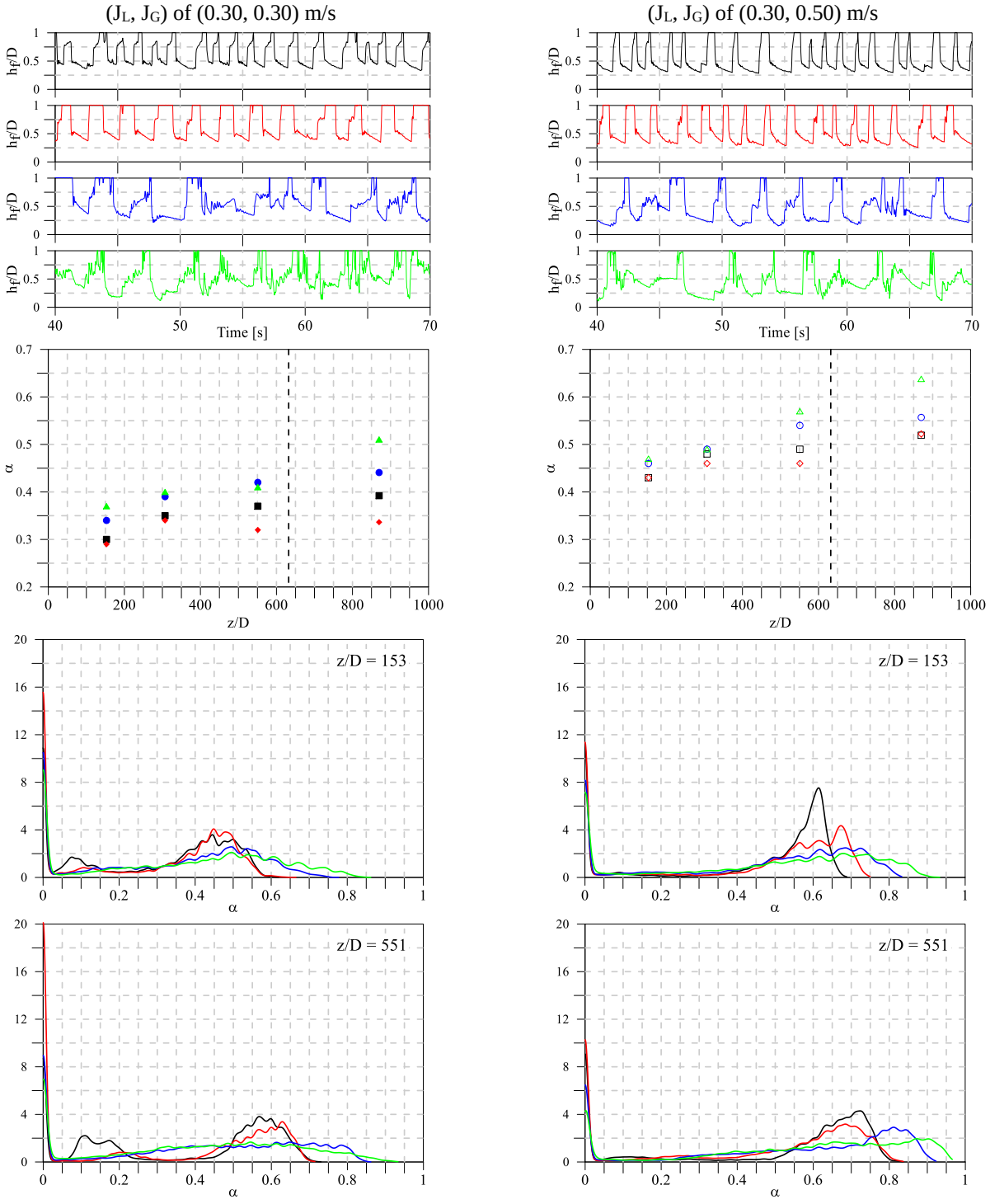

Figure 3. From top to bottom rows: dimensionless liquid film height, h_f/D at S3 for σ of 1.000, 0.250, 0.123 and 0.072; average cross section void fraction along the test section; the next two rows display the PDF of the cross section void fraction at S1 and S3. The symbols and/or the colors □, ◊, o, Δ correspond to area contraction ratios of 1, 0.250, 0.123 and 0.072 respectively. The dashed line represents the axial location of the orifice plate.

Using the PSD, it is possible to disclose the dominant frequencies of the orifice pressure difference and of the h_f/D to cross check the similarity with the frequency of passage of slug units. The PSD data for orifice with σ of 0.250 shown on the 1st row of Figure 5, have dominant frequencies of 0.37 Hz and 0.46 Hz for the left and right columns

respectively. These dominant frequencies disclosed by the PSD processing has no match to the average frequencies of passage shown on the 1st row of Figure 4 graphs' as well as on Table 2 but a match is found if one looks at the modes of the PDFs shown on the 2nd row of Figure 4. For the left column data of Figure 4, the PDF mode for σ of 0.250 at S1 and S3 has a match from the PSD dominant frequency by 0.38 Hz at Figure 5, while for the right column data the mode estimates is offset by 0.05 Hz at S1 and S3. These data show a clear correlation between the frequency of passage of slug units and the frequency of pressure pulses. It also indicates the conservation of the slug flow properties, i.e., the lengths and the frequencies of the units are not destroyed up to the orifice.

The PSD data for orifice with σ of 0.072 is shown on the 2nd row of Figure 5. Analyzing the left column data, the spectrum of frequencies is in opposition to the previous case. The dominant frequencies of the pressure difference at the orifice do not match the dominant frequencies found on the h_f/D spectrum neither at S3 nor at S1. This indicates that the slug flow properties are changing continuously as the air-water mixture approaches the orifice. The data on the pressure difference at the orifice and on h_f/D traces on the right column show a partial match against the dominant frequencies. At S3, the spectrums share in common the frequencies 0.24 Hz, 0.30 Hz and 0.35 Hz and the frequency of passage of 0.30 Hz at S3 determined by the PDF mode on Figure 4. On the other hand, the PSD shared frequencies with the orifice pressure difference, and h_f/D at S1 and S3, simultaneously are only 0.24 Hz and 0.35 Hz. Furthermore, these common frequencies do not match the frequency of passage of the slugs at S1 and S3, which are of 0.50 Hz and 0.30 Hz, respectively. These values come from the PDF mode shown in Figure 4. The lack of match between the frequency of passage and the spectrum of h_f/D indicate a changing flow structure, which will be addressed on the next section.

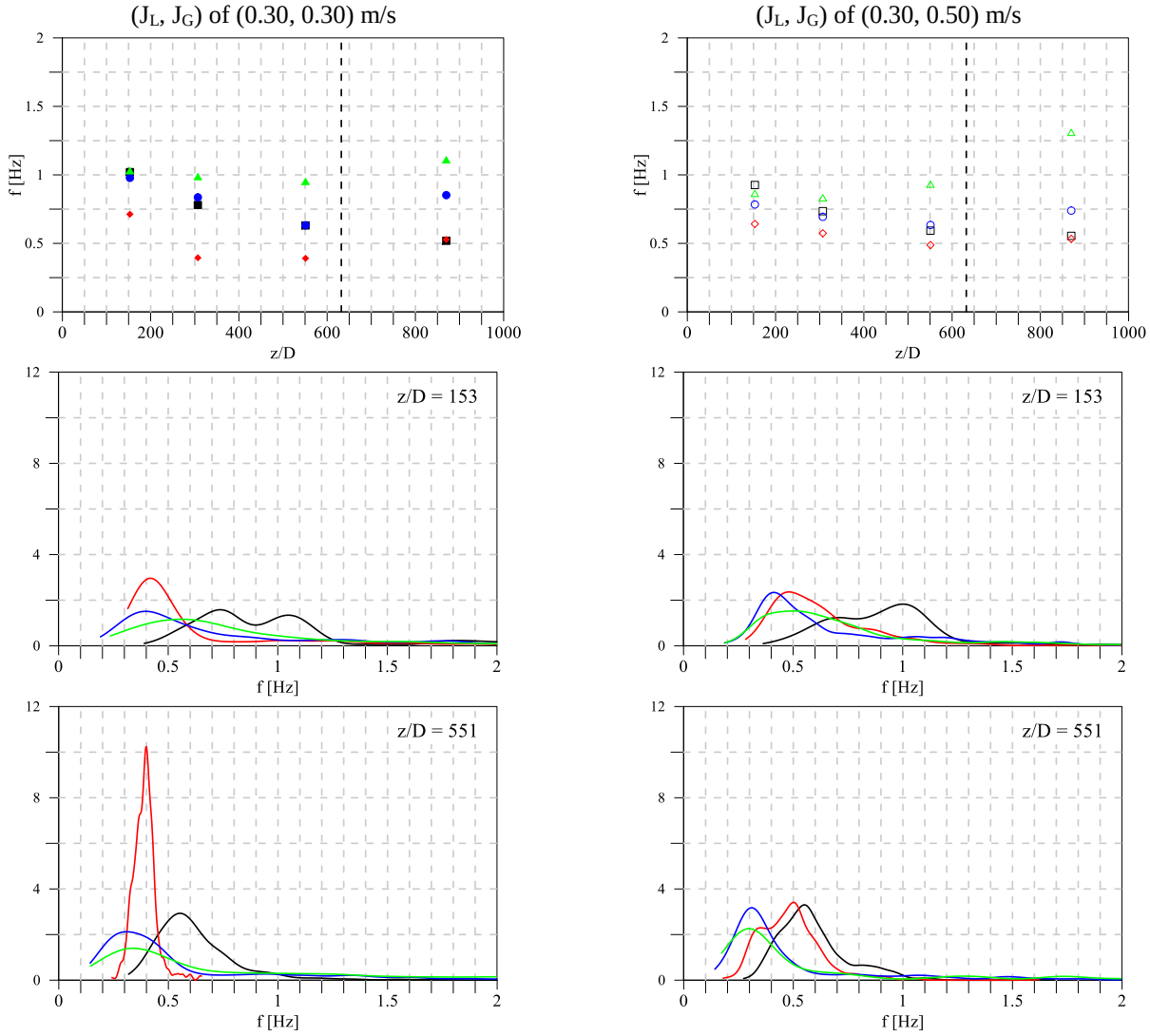

Figure 4. From top to bottom rows: average slug frequency of passage along the test section; the last two rows display the PDF of the slug frequency at S1 and S3. The symbols and/or the colors □, ◊, o, Δ correspond to area contraction ratios of 1, 0.250, 0.123 and 0.072 respectively. The dashed line represents the axial location of the orifice plate.

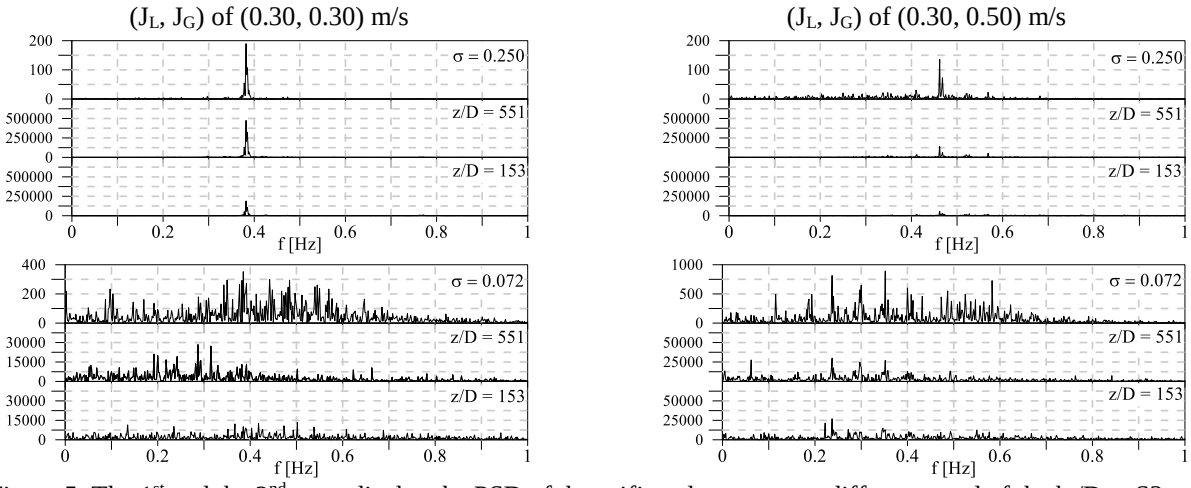

Figure 5. The 1st and the 2nd rows display the PSD of the orifice plate pressure difference and of the h_f/D at S3 and S1 for σ of 0.250 and 0.072, respectively.

3.4 Bubble Nose Translational Velocity

The bubble nose translational velocity is on Figure 6. The figure displays the information using three rows and two columns. The left and right columns refer to data taken with the phases' velocities (J_L, J_G) of (0.30, 0.30) m/s and (0.30, 0.50) m/s respectively. The top row displays average translational velocity, u_T, along the test section. The 2nd row shows the PDF of u_T and the bottom row exhibits the slip ratio along the test section.

Considering the reference case with σ of 1.0, the bubble nose translational velocity is nearly constant along the test section. The u_T values stay within 0.76 m/s to 0.79 m/s and 0.95 m/s to 0.96 m/s for the data on the left and right columns, see local values on Table 2. An exception occurs on the left column data at S1 where it is found u_T of 0.84. This is due to the slug initiation process which the faster bubbles are overtaking the slow ones, therefore we observe a higher velocity. The influence of the obstruction on u_T is developed next only for the measuring stations upstream the orifice plate. Starting with the orifice with σ of 0.250 is observed that u_T stays at S1 through S3 within 0.69 m/s to 0.71 m/s as uniform as the reference data but 9.6% slower. The observed uniformity of u_T from S1 to S3 is due to the high coalescence ratio for this case leading to a quick establishment of the stationary state. The differences on u_T rise for orifices with σ of 0.123 and 0.072. They start with u_T at 153D nearly equal to the reference value of 0.84 m/s but evolve along the test section exhibiting a growing behavior.

The growing behavior of average bubble nose translational velocity is better understood inspecting the PDF of u_T at S3 shown on the 2nd row of Figure 6. The analysis starts with the data belonging to the left column. An inspection on the reference data (σ of 1.0), one finds out that at S3 the u_T PDF is symmetric with high kurtosis indicating the approach of a stationary state. The data for orifice with σ of 0.250 has a PDF skew positive. The shift toward the higher velocities is understood as an effect caused by the orifice. A mixture with low and high void fraction flows through the orifice causing a cyclic pressure increase and decrease, which has a net effect of decelerate or accelerate the mixture. This effect is clearly seen on u_T PDFs for orifices with σ of 0.123 and 0.072, which are bimodal with the high and low velocities being represented by the high and low modes' values. Once again, the bimodal PDFs make the average value loose the physical representativeness. Using the data on the left column as an example, for z/D of 551, one finds for orifices with σ of 0.123 and 0.072 u_T average values of 0.87 m/s and 1.03 m/s while the low and high mode values are (0.6 , 1.05) m/s and (0.6, 1.35) m/s respectively.

The coalescence values on Table 2 disclose a low coalescence rate for flow through orifices with σ of 0.123 and 0.072. To sustain low coalescence rate with large u_T spread, as observed on the u_T PDFs, the only possibility is that these u_T values do not coexist at the same time within the test section. The alternate passage of low and high void fraction mixture through the orifice, causes pulses with low and high pressures, which accelerate and decelerate liquid slugs. Once the maximum velocity of the liquid slug ahead of it drives the bubble nose velocity, (Polonsky, 1999), it is possible to associate the large spread of u_T with an equally large spread of mixture velocity. Lastly, it is introduced the slip ratio as a form to complement this section information disclosing the slip ratio, S, defined as:

$$S = \frac{U_G}{U_L} \equiv \frac{J_G}{J_L}\frac{(1-\alpha)}{\alpha} \tag{7}$$

The estimates of the slip ratio along the test section axial length are displayed on the 3rd row of Figure 6. The analyses are applied to 153 < z/D < 551, i.e., upstream the orifice plate. The slip ratio behavior for σ of 1.0 and 0.250 are similar up to S2, beyond S2, the slip ratio for σ of 1.0 decays while for σ of 0.250 slightly grows in a mirror image of the void fraction shown on Figure 3, left column and 2nd row, the same arguments given at section 3.2 applies here.

For orifices with σ of 0.123 and 0.072, the slip ratios are lower than the reference data and have a trend to decrease as z/D increases. The range of the slip ratio values is similar to the values reported in Fossa et al. (2006) and Fossa and Guglielmini (2002).

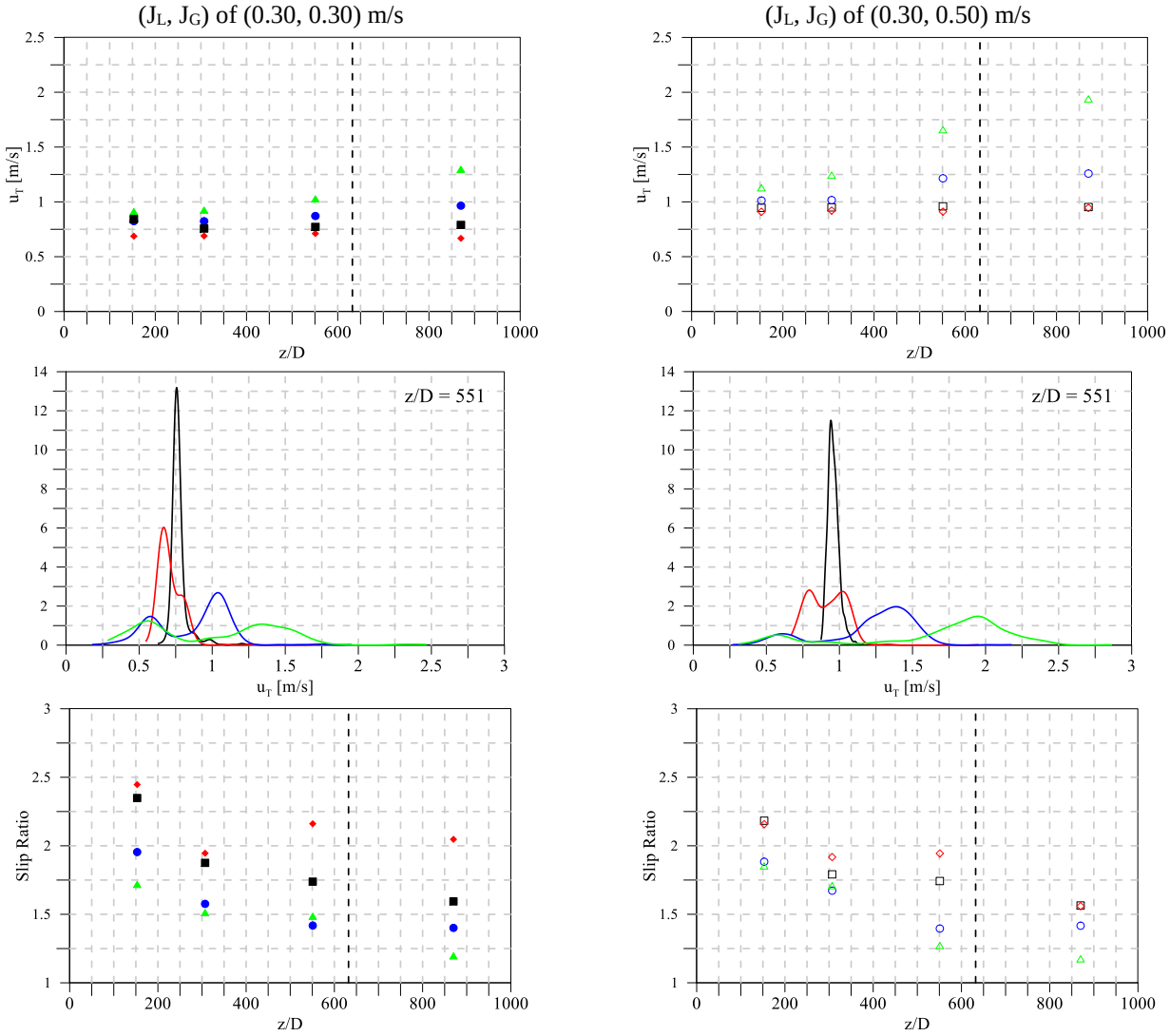

Figure 6. The average bubble nose translational velocity along the test section; the PDF of bubble nose translational velocity at S3 and slip ratio as a function of the pipe axial distance. The symbols and/or the colors □, ◊, o, Δ correspond to area contraction ratios of 1, 0.250, 0.123 and 0.072 respectively. The dashed line represents the axial location of the orifice plate.

3.5 Liquid Film and Liquid Slug Lengths

The average liquid film and liquid slug lengths are on Table 2 for the reference data as well as for the three orifices employing the two pairs of liquid and gas velocities. These data are not presented on a scatter plot but the general trend of L_f/D and L_S/D is to increase as z/D increases. This trend applies to the data laying upstream the orifice. Considering L_f/D properties, the lowest values are found for the reference data, σ of 1, followed, in crescent order, to data belonging to orifices with σ of 0.250, 0.123 and 0.072. The average liquid slug length at 153D downstream the mixer starts with nearly the same values for all tested conditions but as it advances to S2 and S3 they change but do not keep a crescent order. It depends on the axial position, orifices sizes and gas and liquid flow rates.

The behavior of L_f/D and L_S/D is better appraised employing the associated PDF. Figure 7 presents the L_f/D and L_S/D PDFs at S3 on the 1st and 2nd rows. The left and right columns refer to data taken with the phases' velocities (J_L, J_G) of (0.30, 0.30) m/s and (0.30, 0.50) m/s, respectively. Having as reference the L_f/D and L_S/D PDFs for σ of 1, one observes a clear distinction among the PDF shapes. For orifices with σ of 0.250, they are similar to the reference PDF but for orifices with σ of 0.123 and 0.072, they are skew positive with a large spread. Such large and small lengths do

not coexist simultaneously at the test section based on the analysis done for the u_T PDF. The cyclic acceleration and deceleration due to the pressure pulses changes the liquid film length and the void fraction. As the bubble nose is accelerated, the thickness of the associated liquid film decreases; to conserve the mass of gas the film length is reduced. On the other hand, for a deceleration cycle, the liquid film becomes thicker and to conserve the mass of gas, the bubble length increases. These cyclic changes continuously change the lengths of liquid film and liquid piston in time.

The influence of the acceleration and deceleration cycles is visualized on the h_f/D traces for orifices with σ of 0.123 and 0.072 shown on Figure 3. These orifices induce large acceleration cycles due to the low area contraction ratio, which cause the liquid film thinning and thickening as shown on the Figure 3 .

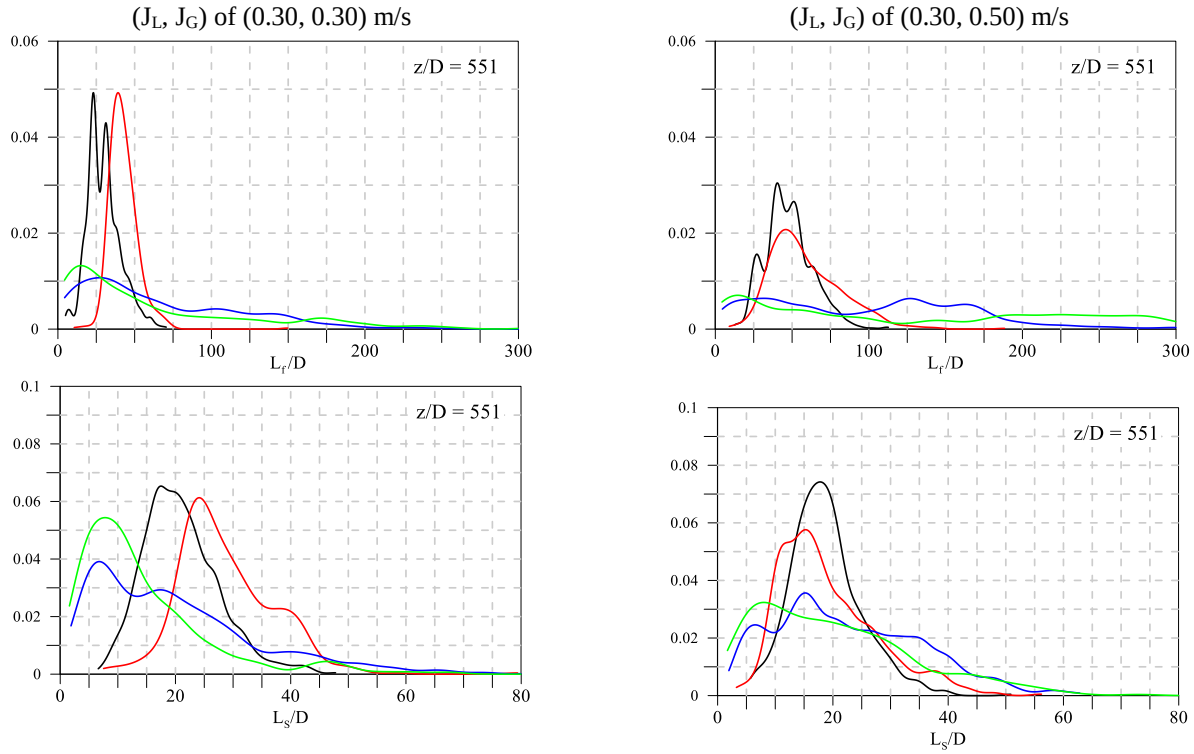

Figure 7. The PDFs of L_f/D and L_S/D at S3. The colors black, red, blue and green correspond to area contraction ratios of 1, 0.250, 0.123 and 0.072 respectively.

4. CONCLUSIONS

The upstream influence of an orifice plate on the horizontal slug flow was studied. The orifice plate has two effects on the slug flow. The first one is the area contraction, inducing at the upstream vicinity of the orifice a flow acceleration continuously deforming the interfaces, changing the slip velocity and the slug flow structure. The second one regards to the pressure pulses back propagated from the orifice plate. The intermittent passage of low and high void fraction mixture through the orifice causes pulses with low and high pressures, which accelerate and decelerate liquid slugs. These pressure pulses have a far-reaching effect on the slug flow properties. At the present study, the pressure pulses interfered at the flow inlet, at 632 D upstream the orifice plate, by changing the slug initiation process, increasing and decreasing the liquid film and slug lengths.

The present experimental data disclose that orifices with area contraction ratio of 0.250 produce weak pressure pulses, which induce weak cycles of acceleration and deceleration, but are capable to reach the pipe inlet at 632 D upstream the orifice plate and modify the slug initiation process. For orifices with lower area contraction of 0.123 and 0.072, were also detected changes on the slug initiation and experienced strong pressure pulses. The liquid film submitted to the acceleration cycles has a tendency to increase the film length and decrease the void fraction during the acceleration phase and the opposite during the deceleration phase. Visual observation during the deceleration phase showed bubble break up and the rise of short liquid slugs. The rise of new liquid slugs and liquid films with different sizes are responsible for generating a large spectrum of frequency as seen on the experimental data.

5. REFERENCES

Ahmed, W. H., Ching, C. Y., & Shoukri, M., 2008. “Development of two-phase flow downstream of a horizontal sudden expansion”. International Journal of Heat and Fluid Flow, 29(1), 194-206.

Aloui, F., Doubliez, L., Legrand, J., & Souhar, M., 1999. "Bubbly flow in an axisymmetric sudden expansion: Pressure drop, void fraction, wall shear stress, bubble velocities and sizes". Experimental thermal and fluid science, 19(2), 118-130.

Bertola, V., 2004. "The structure of gas-liquid flow in a horizontal pipe with abrupt area contraction". Experimental thermal and fluid science, 28(6), 505-512.

Chen, Y., Chu, M. C., Liaw, J. S., & Wang, C. C., 2008. "Two-phase flow characteristics across sudden contraction in small rectangular channels". Experimental Thermal and Fluid Science, 32(8), 1609-1619.

Chisholm, D., 1983. "Two-phase flow in pipelines and heat exchangers" (p. 110). London: George Godwin.

Dalla Maria, L., 2016. "Estudo Experimental das Ondas de Fração de Vazio e Pressão em Escoamento Horizontal Transiente de Ar e Água no Padrão Intermitente". Master's thesis, Universidade Estadual de Campinas, Campinas, SP, Brazil.

Fossa, M., & Guglielmini, G., 1998. "Dynamic void fraction measurements in horizontal ducts with sudden area contraction". International journal of heat and mass transfer, 41(23), 3807-3815.

Fossa, M., & Guglielmini, G., 2002. "Pressure drop and void fraction profiles during horizontal flow through thin and thick orifices". Experimental Thermal and Fluid Science, 26(5), 513-523.

Kojasoy, G., Landis, F., Kwame-Mensah, P., & Chang, C. T., 1997. "Two-phase pressure drop in multiple thick-and thin-orifice plates". Experimental thermal and fluid science, 15(4), 347-358.

Lin, Z. H., 1982. "Two-phase flow measurements with sharp-edged orifices". International Journal of Multiphase Flow, 8(6), 683-693.

Lush, P. A., & Skipp, S. R., 1986. "High speed cine observations of cavitating flow in a duct". International journal of heat and fluid flow, 7(4), 283-290.

Oliveira, J. L. G., Passos, J. C., Verschaeren, R., & van der Geld, C., 2009. "Mass flow rate measurements in gas-liquid flows by means of a venturi or orifice plate coupled to a void fraction sensor". Experimental Thermal and Fluid Science, 33(2), 253-260.

Petrick, M., & Swanson, B. S., 1959. "Expansion and contraction of an air-water mixture in vertical flow". AIChE Journal, 5(4), 440-445.

Polonsky, S., Shemer, L., & Barnea, D., 1999. "The relation between the Taylor bubble motion and the velocity field ahead of it". International Journal of Multiphase Flow, 25(6), 957-975.

Rosa, E. S., Salgado, R. M., Ohishi, T., & Mastelari, N., 2010. "Performance comparison of artificial neural networks and expert systems applied to flow pattern identification in vertical ascendant gas–liquid flows". International Journal of Multiphase Flow, 36(9), 738-754.

Salcudean, M., Groeneveld, D. C., & Leung, L., 1983. "Effect of flow-obstruction geometry on pressure drops in horizontal air-water flow". International Journal of Multiphase Flow, 9(1), 73-85.

Schmidt, J., & Friedel, L., 1997. "Two-phase pressure drop across sudden contractions in duct areas". International journal of multiphase flow, 23(2), 283-299.

Taitel, Y., & Barnea, D., 1990. "Two-phase slug flow". Adv. Heat Transfer, 20, 83-132.

Talvy, C. A., Shemer, L., & Barnea, D., 2000. On the interaction between two consecutive elongated bubbles in a vertical pipe. International Journal of Multiphase Flow, 26(12), 1905-1923.

Thang, N. T., & Davis, M. R., 1981. "Pressure distribution in bubbly flow through venturis". International Journal of Multiphase Flow, 7(2), 191-210.

Zuber, N., & Findlay, J. A., 1964. "The effects of non-uniform flow and concentration distributions and the effect of the local relative velocity on the average volumetric concentration in two-phase flow". (No. GEAP-4592; EURAEC-1096). General Electric Co., Schenectady, NY.

6. RESPONSIBILITY NOTICE

The authors are the only responsible for the printed material included in this paper.